Maximum output power of broad–area laser diodes

(Invited Paper)

H. Wenzel, P. Crump, A. Pietrzak, C. Roder, R. Staske, X. Wang and G. Erbert
Ferdinand–Braun–Institut für Höchstfrequenztechnik
Gustav–Kirchhoff-Str. 4
12489 Berlin
Germany

***Abstract*—The causes for the saturation of both the continuous–wave and the pulsed output power of broad–area laser diodes driven at very high currents are investigated experimentally and theoretically. The decrease of the gain due to self–heating under continuous–wave operation and spectral holeburning and carrier heating under pulsed operation as well as hetero–barrier carrier leakage and longitudinal spatial holeburning are the dominating mechanisms limiting the maximum achievable output power.**

I. Introduction

High–power laser diodes are the root source of optical energy in all high performance laser systems. Broad–area diode lasers (either as single emitters or in bars) are in wide–spread application in part because of their ease of fabrication. In recent years, their output power was driven to higher and higher values by steadily increasing the efficiency. In principle the maximum achievable power is limited by the damage threshold of the semiconductor crystal (catastrophic optical damage, COD), either within the laser cavity or at the facets. However, different measures like the reduction of the power density by broadening the optical waveguide [1], the improvement of the crystal quality [2] and special facet treatments [3] significantly extended the COD power. Thus increasingly physical effects like self–heating [4], carrier leakage [5] and gain compression [6] limit the achievable power. In this talk we will present results of two–dimensional simulations of the vertical carrier transport, heat flow, and waveguiding accounting for hetero–barrier leakage, longitudinal spatial holeburning (LSH) and spectral holeburning (SHB). Lateral effects like filamentation and thermal lensing were dropped. We will consider both continuous–wave operation and pulsed operation, where the self–heating of the lasers can be neglected, and compare the results to measurements.

II. Model

The simulations are based on the "Treat Power as a Parameter"(TPP) method as explained in [7] and [8]. In Fabry–Perot lasers as investigated here, the forward and backward propagating optical power P^+ and P^- solve the equations

$$\pm\frac{dP^\pm}{dz} = \Big\{g_m(U,P)/\big[1+P/P_\mathrm{s}\big] - \alpha_0\Big\}P^\pm \qquad (1)$$

subject to the boundary conditions

$$P^+(0) = R_0P^-(0) \quad \text{and} \quad P^-(L) = R_LP^+(L), \qquad (2)$$

TABLE I
Layer sequence, thicknesses and ionized doping densities of the structure under study

layer	compound	thickness / nm	doping / 10^{18} cm^{-3}
cladding	p-$Al_{0.25}Ga_{0.75}As$	25	-2.
GRIN	GaAs → p-$Al_{0.25}Ga_{0.75}As$	1500	-0.1 → -2.
confinement	p-GaAs	800	-0.05
		100	-0.01
spacer	GaAs	10	
QW	$In_{0.29}Ga_{0.71}As$	7	
barrier	GaAs	50	
QW	$In_{0.29}Ga_{0.71}As$	7	
barrier	GaAs	50	
QW	$In_{0.29}Ga_{0.71}As$	7	
barrier	GaAs	50	
QW	$In_{0.29}Ga_{0.71}As$	7	
spacer	GaAs	10	
confinement	n-GaAs	1300	0.01
		100	0.1
		200	0.2
		500	0.5
cladding	p-$Al_{0.25}Ga_{0.75}As$	100	0.5
		100	1

and where

$$P(z) = P^+(z) + P^-(z) \qquad (3)$$

is the total power. The modal gain g_m is twice the imaginary part of the propagation constant β which is obtained as a solution of the vertical waveguide equation

$$\Big[\frac{d^2}{dx^2} + \frac{4\pi^2}{\lambda^2}\varepsilon(n,p,T,x) - \beta^2\Big]E(x) = 0, \qquad (4)$$

where

$$\varepsilon = \big[n + i\lambda(g-\alpha)/(4\pi)\big]^2 \qquad (5)$$

with n being the refractive index, g the local gain and α the local absorption coefficient.. The electron and hole densities n and p as well as the temperature distribution T are solutions of the vertical drift–diffusion and heat–flow equations. For this, the simulation tool WIAS–TeSCA [9] is used. More details on material functions and boundary conditions will be given at the conference.

As result of the simulation in the vertical direction, g_m is obtained as a function of the bias U and the local power P. In Eq. (1) α_0 comprises scattering and radiation losses

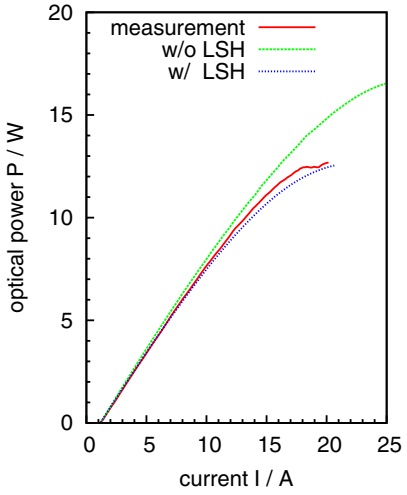

Fig. 1. CW power–current characteristics. Red solid line: measurement, green dashes and blue short dashes: simulation without and with, respectively, longitudinal spatial holeburning.

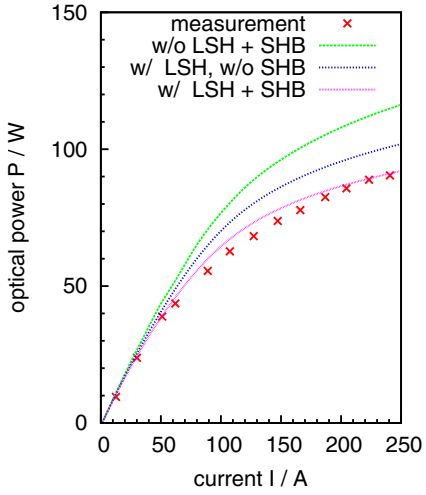

Fig. 2. Pulsed power–current characteristics. Red crosses: measurement, green dashes and blue short dashes: simulation without and with, respectively, longitudinal spatial holeburning. Magenta dots: simulation with spectral holeburning included.

not contained in α and P_s is a saturation power describing phenomenologically gain compression caused by spectral holeburning and carrier heating (denoted by SHB) [10]. LSH is accounted for via the power dependence of g_m in Eq. (1). If the term in the braces of Eq. (1) is evaluated at the average power in the cavity, the usual model neglecting LSH is recovered.

III. Device parameters

The layer sequence, thicknesses and ionized doping densities of the structure under study are compiled in Tab. 1. The epitaxial layer structure was grown on a n–GaAs substrate. The emission wavelength is $\lambda \propto 1060$ nm. Cavity length and stripe width are $L = 4$ mm and $W = 100$ μm, respectively, and the facet reflectivities are $R_0 = 0.01$ and $R_L = 0.95$. For CW operation, the laser diode was mounted on a conductively cooled package.

IV. Results

Figs. 1 and 2 show the measured and simulated power–current characteristics under CW and pulsed, respectively, operation of two laser diodes. Experimentally, a maximum CW output power of $P = 13$ W limited by thermal rollover and a maximum pulsed output power of $P = 90$ W limited by the current driver were achieved. Thermal rollover is caused by the decrease of the gain due to internal self–heating and increased hetereo–barrier leakage. However, as Fig. 1 reveals, good agreement between measurement and simulation is achieved only if longitudinal spatial holeburning (LSH) is taken into account. Under operation with short current pulses (300 ns pulse width), self–heating can be almost neglected. Due to the high power reached now gain compression affects the power–current characteristics. Therefore, besides LSH, a finite saturation power $P_s = 300$ W has to be taken into account in order to obtain sufficiently good agreement between measurement and simulation (Fig. 2). This saturation power corresponds to a gain compression factor of approximately 10^{-23} m^{-3}, which is on the lower limit of the values given in [10]. More insight into the physics and results for longer cavity lengths as well as other layer structures will be presented at the conference.

References

[1] G. Erbert, F. Bugge, B. Eppich, J. Fricke, K.-H. Hasler, K. Paschke, A. Pietrzak, H. Wenzel, G. Tränkle, "High brightness diode lasers with very narrow vertical divergence," *Proc. SPIE*, vol. 6909, p. 69090P, 2008.

[2] F. Bugge, U. Zeimer, R. Staske, B. Sumpf, G. Erbert and M. Weyers, "MOVPE growth optimization for laser diodes with highly strained InGaAs MQWs," *J. Crystal Growth*, vol. 298, pp. 652-657, 2007.

[3] P. Ressel, G. Erbert, U. Zeimer, K. Hausler, G. Beister, B. Sumpf, A. Klehr, G. Tränkle, "Novel passivation process for the mirror facets of Al–free active–region high–power semiconductor diode dasers," *IEEE Photon. Techn. Lett*, vol. 17, pp. 962–964, 2005.

[4] P. Crump, G. Blume, K. Paschke, R. Staske, A. Pietrzak, U. Zeimer, S. Einfeldt, A. Ginolas, F. Bugge, K. Häusler, P. Ressel, H. Wenzel, G. Erbert, "20W continuous wave reliable operation of 980nm broad–area single emitter diode lasers with an aperture of 96μm, " *Proc. SPIE*, vol. 7198, p. 719814, 2009.

[5] A. Pietrzak, P. Crump, H. Wenzel, R. Staske, G. Erbert, G. Tränkle, "55 W peak power from 1100 nm wavelength 60 μm broad–area laser diodes enabled by reduced carrier accumulation in the waveguide," *Semicond. Sci. Technol.*, vol. 24, p. 035020, 2009.

[6] S. O. Slipchenko, Z. N. Sokolova, N. A. Pikhtin, K. S. Borschev, D. A. Vinokurov, I. S. Tarasov, "Finite time of carrier energy relaxation as a cause of optical–power limitation in semiconductor lasers," *Semiconductors*, vol. 40, p. 990, 2006.

[7] H.J. Wünsche, U. Bandelow, H. Wenzel, "Calculation of combined lateral and longitudinal spatial hole burning in $\lambda/4$ shifted DFB lasers," *IEEE J. Quantum Electron.*, vol. 17, pp. 1751–1760, 1993.

[8] H. Wenzel, G. Erbert, "Simulation of single–mode high–power semiconductor lasers," *Proc. SPIE*, vol. 2693, p. 418, 1996.

[9] U. Bandelow, H. Gajewski, R. Hünlich, "Fabry–Perot lasers: Thermodynamics–based modeling," in: *Optoelectronic Devices – Advanced Simulation and Analysis*, J. Piprek, Ed., New York: Springer, pp. 63–85, 2005.

[10] J. Wang, H.C. Schweizer, "A quantitative comparison of the classical rate–equation model with the carrier heating model on dynamics of the quantum–well laser, " *IEEE J. Quantum Electron.*, vol. 33, pp. 1350–1358, 1997.